


 Cite this: *RSC Adv.*, 2025, 15, 43665

Silver doped copper oxide decorated graphene oxide nanocomposite for electrochemical sensing, photocatalysis and biomedical applications

 Asmaa M. Alghamdi ^a and Abid Ali *^b

A silver-doped copper oxide nanocomposite decorated on graphene oxide (Ag–CuO@GO) was synthesized *via* a facile wet-chemical method and characterized using XRD, SEM, FTIR, UV-vis, and EDX analyses. The synergistic combination of Ag and CuO onto GO provided greater charge separation, better conductivity, and a high surface-area framework for uniform nanostructure distribution. Electrochemical studies confirmed excellent sensing performance toward dopamine, with rapid electron transfer kinetics and a low limit of detection (23.6 μM) and higher sensitivity of 3.43 $\text{mA cm}^{-2} \text{mM}^{-1}$. Correspondingly, photocatalytic studies revealed that Ag–CuO@GO showed remarkable dye degradation capability. Ag–CuO@GO achieved up to 96% degradation of MB under direct sunlight with 0.3 mg mL^{-1} catalyst loading in 30 minutes. While kinetic studies at 0.2 mg mL^{-1} followed pseudo-first-order kinetics with an apparent rate constant of 0.019 min^{-1} . Additionally, due to the intrinsic biomedical properties of Ag and CuO, the nanocomposite also exhibits notable antibacterial activity, further broadening its potential practical utility. These results confirm Ag–CuO@GO as an efficient multi-functional material for electrochemical sensing, photocatalytic degradation of organic dyes and antibacterial activity.

Received 25th September 2025

Accepted 15th October 2025

DOI: 10.1039/d5ra07285a

rsc.li/rsc-advances

1 Introduction

The emergence of multidimensional nanomaterials has significantly advanced the development of multifunctional platforms for biomedical, environmental, electrochemical and photocatalytic applications.^{1,2} Among these, hybrid nanocomposites incorporating metal oxides, noble metals,³ where carbon-based supports have demonstrated exceptional physicochemical and functional properties.⁴ Copper oxide (CuO), a p-type semiconductor with a narrow band gap (~ 1.2 – 1.9 eV), has garnered attention for its inherent redox activity, catalytic efficiency, cost-effectiveness, and biocompatibility.^{5,6} However, its practical use is often constrained by limited surface area, agglomeration, and suboptimal charge separation.⁷ To overcome these drawbacks, the integration of CuO with other functional components is essential.⁸

Doping with silver nanoparticles (Ag NPs) has proven to be a powerful strategy to boost CuO's photocatalytic and bactericidal activity.⁹ Owing to their strong surface plasmon resonance (SPR), electrical conductivity, and ion-releasing behavior, Ag NPs impart superior charge separation and antimicrobial efficiency when coupled with CuO.^{10,11} Additionally, graphene oxide (GO), a highly oxidized derivative of graphene, offers a large surface area, abundant oxygenated functional groups, and

excellent dispersibility in aqueous media.¹² GO not only enhances the mechanical stability and dispersion of metal/metal oxide nanoparticles but also promotes interfacial charge transfer, making it an ideal scaffold for nanohybrid architectures.^{13,14} In this context, the design of an Ag-doped CuO nanostructure anchored onto graphene oxide (GO) sheets (Ag–CuO@GO) presents a promising route to developing multifunctional nanomaterials.¹⁵ Such composites are expected to exhibit enhanced antimicrobial properties due to the synergistic interplay between Ag⁺-induced membrane disruption, CuO-mediated oxidative stress, and GO's ability to trap and anchor microbial cells.^{11,16} In the context of photocatalytic application, Ag–CuO@GO nanostructure could enhance the photocatalytic activity by facilitating efficient charge separation and transfer to and from the electrolyte and electrode, where Ag acts as an electron sink, CuO absorbs visible light, and GO provides a high-surface-area conductive support.¹⁷ Moreover, the hybrid framework offers an electroactive surface suitable for the sensitive detection of biologically relevant analytes, such as dopamine (DA),¹⁸ a key neurotransmitter involved in numerous physiological processes.^{19,20}

Dopamine is an essential neurotransmitter that requires accurate detection because aberrant levels are associated with neurological conditions including schizophrenia and Parkinson's. Because of its redox activity, it is perfect for electrochemical sensing with Ag–CuO@GO and other nanostructured materials.²¹ Electrochemical sensing platforms based on nanostructured electrodes offer rapid, selective, and low-cost

^aFaculty of Science, Department of Biology, Al-Baha University, Al-Baha, Saudi Arabia

^bDepartment of Chemistry, The University of Lahore, 1-Km Defence Road, Lahore, 54590, Pakistan. E-mail: abid.ali@chem.uol.edu.pk


solutions for real-time monitoring of biomolecules.²² For ultrasensitive sulfadimethoxine detection, a ternary Z-scheme/type-II heterojunction based on BiOCl/BiO₃/BiOI allowed for improved charge separation and PEC response. A strong basis for food safety monitoring in intricate samples is provided by this design.²³ Methylcellulose hydrogels supplemented with GO@Fe₃O₄ demonstrated improved electron transitions and energy band gap tuning, as well as improved optical and antibacterial capabilities. These multipurpose nanocomposites show promise for use in optoelectronic and biological applications of the future.²⁴ The integration of Ag–CuO along with GO can further amplify the sensing response through efficient electron transfer and high catalytic activity.²⁵ Recent studies have demonstrated the individual potential of Ag,²⁶ CuO,²⁷ and GO in biosensing and antibacterial applications;^{28,29} however, reports on their ternary hybrid systems with multi functionality remain limited.³⁰

The present work addresses this gap by synthesizing a novel Ag–CuO@GO nanocomposite through a facile co-precipitation route followed by thermal treatment.³¹ The structural and morphological features were comprehensively characterized using XRD, SEM, EDX, FTIR, and UV-vis techniques. Electrochemical behavior of Ag–CuO@GO was evaluated *via*, cyclic and square wave voltammetry along with chronoamperometric studies using dopamine as a model analyte, while photocatalytic activity was assessed using MB dye. Moreover, its antibacterial performance was assessed against *E. coli* and *S. aureus* using disc diffusion assays. This study not only highlights the importance of material design in enhancing electrochemical transduction but also establishes a clear correlation between nanoscale architecture and antimicrobial efficacy. The combination of Ag doping, CuO semi-conductivity, and GO support confers the nanocomposite with superior physicochemical stability, rapid electron kinetics, and broad-spectrum antimicrobial action. These results suggest that the Ag–CuO@GO composite holds substantial promise as a multi-function material for future deployment in bioanalytical sensors, antimicrobial coatings, and water treatment technologies.

2 Experimental section

2.1 Materials

Graphene, copper chloride dihydrate (CuCl₂·2H₂O), silver chloride (AgCl) and trisodium citrate (Na₃C₆H₅O₇) were obtained from Sigma-Aldrich and used without further purification. Distilled water was employed throughout all solution preparations. Sodium hydroxide (NaOH) and ethanol were purchased from Merck. GAMRY 1010E potentiostat/galvanostat equipped with a three-electrode system-comprising a glassy carbon working electrode, platinum wire counter electrode, and Ag/AgCl (3 M KCl) reference electrode was used for all electrochemical measurements. All glassware was acid-washed and rinsed thoroughly with distilled water before use.

2.2 Synthesis of Ag–CuO@GO nanocomposite

Hydrophobic graphene was functionalized *via* acidic treatment to convert it into its hydrophilic graphene oxide (GO). Sulfuric

acid (5 M) was used in chemical treatment to oxidize graphene into graphene oxide. A standard co-precipitation procedure was used for the synthesis of the silver doped CuO nanoparticles in a regular shape over graphene oxides nanosheets. Briefly, a suspension of 30 mg of GO was dispersed into 50 mL of deionized water under constant stirring. In a separate container 0.1 M (0.85 g) of CuCl₂·2H₂O and 5 mM (35.75 mg) of AgCl was dissolved in 50 mL of deionized water and stir the mixture until a clear solution was achieved. The resulting solution was gradually added to the suspension of GO under constantly stirring. In the next step, trisodium citrate (Na₃C₆H₅O₇) solution (50 mM) has been added in the above mixture and maintain its pH 10 *via* NaOH (2 M) solution added drop by drop. The system was constantly agitated for 10 hours at 60 °C and stayed overnight (24 hours) for the growth of well-ordered structure of silver doped copper oxide over the graphene oxide nanosheets. Finally, the product was collected and washed with ethanol and water several time and dried in an oven at 50 °C.

2.3 Characterization

X-ray diffraction (XRD) analysis was performed using a Bruker D8 Advance Twin-Twin (Cu K) to examine the structural characteristics of Ag–CuO@GO NCs. The surface morphology was observed using scanning electron microscopy (SEM, Quanta FEG-250) to validate the nanostructure formation. Energy-dispersive X-ray spectroscopy (EDX) elemental mapping was performed for elemental confirmation, composition and distribution of Ag, Cu, O, and C. Fourier-transform infrared spectroscopy (FTIR, Bruker Alpha-II, ATR mode) was used to confirm the functional groups present on the surface of the NCs within the range of 4000–500 cm^{−1}.

2.4 Electrochemical studies

Cyclic voltammetry (CV) was performed to evaluate the electrocatalytic performance of the synthesized Ag–CuO@GO nanocomposite. Electrochemical studies were conducted in phosphate buffer solution (PBS, pH 7.0) containing dopamine as the target analyte. A standard three-electrode setup was utilized in electrochemical studies to examine the redox behavior of nanocomposite, while measurements were recorded using a potentiostat/galvanostat (GAMRY 1010E) with the modified glassy carbon electrode (GCE) serving as the working electrode, Ag/AgCl as the reference, and platinum wire as the counter electrode. The CV curves were recorded at varying scan rates to assess the electron transfer kinetics and determine the diffusion-controlled behavior of dopamine oxidation. The glassy carbon electrode (GCE) was polished with alumina slurry followed by rinsed with distilled water as well as ethanol and dried at room temperature. A catalyst ink was prepared by dispersing 0.2 mg of Ag–CuO@GO in ethanol with Nafion as a binder under ultrasonication. Finally, drop casting method applied for the suspension of aliquot onto the GCE surface and dried to obtain the developed electrode (working) for electrochemical studies. All measurements were carried out at room temperature, and the electrode surface was cleaned and polished before each experiment.



2.5 Antibacterial activity assay

The antibacterial activity of Ag–CuO@GO was evaluated against *Escherichia coli* (ATCC 25922) and *Staphylococcus aureus* (ATCC 29213) by applying disk diffusion method. Bacterial suspensions were adjusted to 0.5 McFarland standard and were swabbed homogeneously onto Mueller–Hinton agar plates. Sterile filter paper disks of 6 mm diameter were infused with 5 μL and 10 μL of the Ag–CuO@GO composite solution (1 mg mL^{-1}) and placed onto the inoculated agar. Disks infused with 10 μL of distilled water and streptomycin (1 mg mL^{-1}) served as negative and positive controls, respectively. The plates were incubated at 37 $^{\circ}\text{C}$ for 24 hours, after which the zones of inhibition were measured. All experiments were performed in triplicate.

2.6 Photocatalytic degradation

The photocatalytic activity of Ag–CuO@GO was assessed using methylene blue (MB) dye as a model pollutant under direct sun light irradiation. 20 mg of the nanocomposite was dispersed in 100 mL of 5 ppm MB solution to maintain catalyst concentration of 0.2 mg mL^{-1} . The solution was exposed to a direct sunlight source. Aliquots (3 mL) were collected at regular intervals and centrifuged to remove nanocomposites. Additionally, catalyst concentration effect was studied by varying the catalyst concentration from 0.05 mg mL^{-1} to 0.3 mg mL^{-1} while maintaining dye concentration same. The residual dye concentration was monitored using UV-vis spectroscopy by measuring the absorbance at $\lambda_{\text{max}} = 664 \text{ nm}$. The degradation efficiency and kinetics were calculated using the formulas:

$$\% \text{ Degradation} = \frac{C_0}{C} \times 100 \quad (1)$$

$$\log \frac{C_0}{C} = K_{\text{app}} \times t \quad (2)$$

where C_0 is initial concentration, C is concentration at time interval t and K_{app} is apparent rate constant. The stability of the Ag–CuO@GO composite was evaluated through five consecutive cycles of photocatalytic degradation MB using 0.3 mg mL^{-1} catalyst concentration. After each cycle, the catalyst was recovered by centrifugation at 8000 rpm for 5 minutes, washed thoroughly with deionized water and ethanol, and dried at 80 $^{\circ}\text{C}$ for 1 hour. The recovered catalyst was then reused in a fresh MB solution with the same initial concentration. The degradation efficiency for each cycle was calculated to assess the stability of the catalyst.

3 Results and discussion

3.1 Characterization of Ag–CuO@GO composite

3.1.1 SEM. Fig. 1 illustrates the surface morphologies of the synthesized nanomaterials captured through scanning electron microscopy (SEM) at varying magnifications. Images (a–c) correspond to pristine low-resolution image of CuO nanocubes, where Fig. 1(a) at 10 μm reveals agglomerated nanostructures forming a sponge-like matrix, suggesting a high surface-to-volume ratio beneficial for surface reactions. At higher magnification in Fig. 1(b and c) at 5 μm scale, respectively, the CuO nanoparticles exhibit a denser distribution and more defined granular boundaries, indicating improved crystallinity and uniform growth. In contrast, Fig. 1(d–f) displays the morphological evolution following Ag doping and GO integration with high resolution. In (d) and (e), the emergence of cubic and faceted structures is observed, characteristic of Ag-decorated CuO with enhanced crystalline domains. Notably, Fig. 1(f) captured at 1 μm magnification reveals a heterogeneous

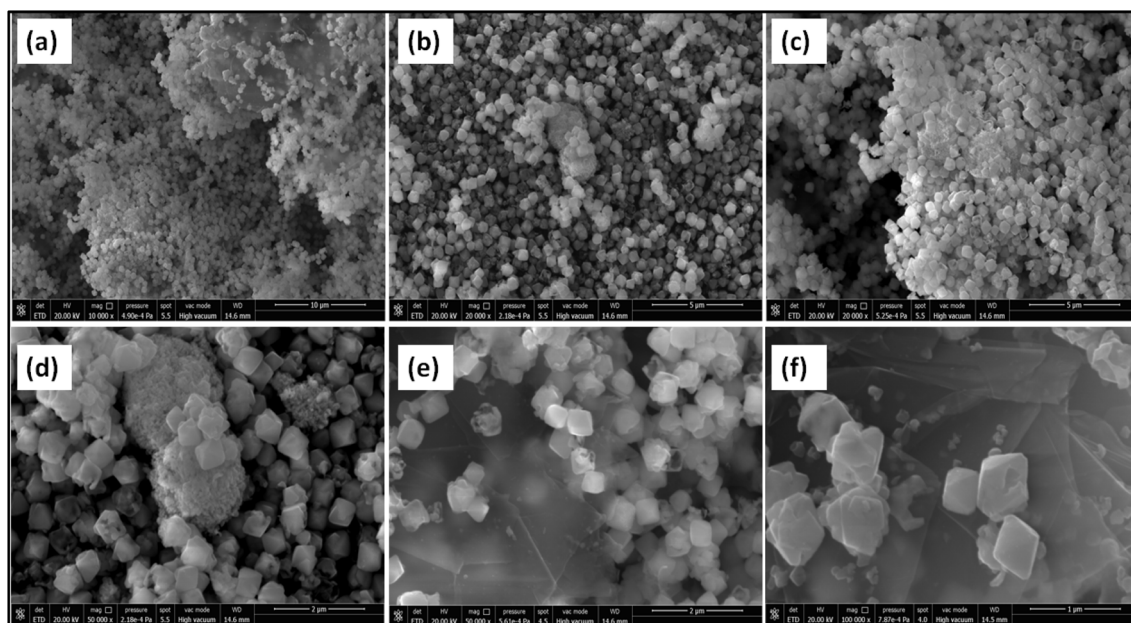


Fig. 1 SEM images for the morphologies of Ag doped CuO@GO with (a–c) lower and (d–f) higher resolution.



visuality, where sharp-edged nano cubes are embedded over layered graphene oxide (GO) sheets.³² This structural arrangement confirms the successful anchoring of Ag–CuO onto GO, offering a favorable hybrid architecture for electrochemical activity due to increased active sites and improved electron transport pathways.

3.1.2 EDX. Energy-dispersive X-ray spectroscopy (EDX) was employed to confirm the elemental composition and spatial distribution of the components in the prepared material.³³ EDX mapping provides localized elemental information, validating the presence and uniform dispersion of key elements throughout the sample surface. Fig. 2(a–e) displays the elemental mapping images obtained *via* energy-dispersive X-ray spectroscopy (EDX), revealing the uniform distribution of elements within the Ag–CuO@GO nanocomposite. The survey analysis in Fig. 2(a) confirms a well-integrated structure, with overlapping signals corresponding to the constituent elements. Fig. 2(b) shows the distribution of carbon, characterized by red coloration, while Fig. 2(c) represents oxygen in green, indicating the presence of the graphene oxide (GO) support. Fig. 2(d) reveals silver as dopant, distributed marked in yellow, affirming the presence of silver as dopant while Fig. 2(e) depicts the copper as most abundant within the fabricated hybrid (Ag–CuO@GO). Elemental distribution is validating the dispersion of each element across the observed area. The mapping data collectively confirms the successful decoration of doped CuO nanoparticles on the GO matrix with homogeneous elemental dispersion, substantiating the composite's morphological and compositional integrity.

3.1.3 XRD. The crystalline integrity and phase identification of the synthesized nanomaterial were investigated using X-ray diffraction analysis.³⁴ As depicted in Fig. 3, the diffractogram of Ag-doped CuO exhibits well-defined peaks, indexed to the monoclinic phase of CuO (JCPDS no. 80-1916),³⁵ with additional minor reflections corresponding to metallic Ag (JCPDS no. 04-0783),³⁶ confirming successful incorporation of silver into the

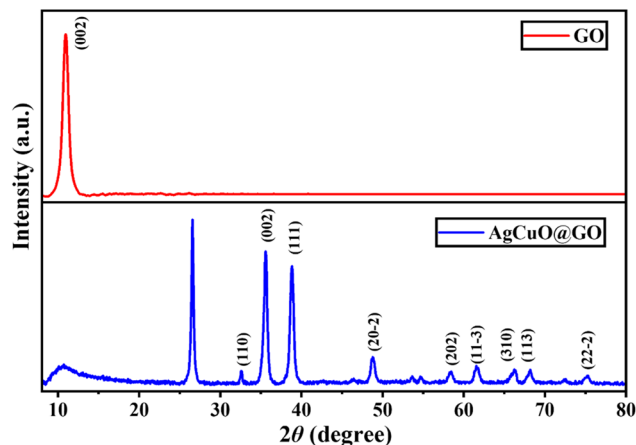


Fig. 3 XRD patterns of graphene oxide (GO) and Ag-doped CuO@GO showing monoclinic CuO phases.

copper oxide lattice. The broad diffraction hump centered around 10.9° observed in the GO sample is characteristic of its amorphous layered structure with oxygenated functionalities.³⁷ Upon hybridization with Ag–CuO, this peak diminishes significantly, indicating a strong interfacial interaction between the GO sheet and the metal oxide nanoparticles. The crystallite size of Ag–CuO was estimated using the Debye–Scherrer formula, yielding average dimensions in the nanometric regime (~18–25 nm),³⁸ indicative of a high surface-to-volume ratio beneficial for photocatalytic and microbial interactions. Moreover, these outcomes validate the successful structural integration of Ag and CuO on the GO matrix, laying the foundation for enhanced charge mobility and antimicrobial performance.

3.1.4 FTIR. Fig. 4 illustrates the Fourier-transform infrared (FTIR) spectra of the synthesized silver doped CuO decorated at graphene oxide (CuO@GO) nanocomposite, spanning the spectral range of 4000–500 cm⁻¹. The GO spectrum (blue trace) displays a series of well-defined peaks indicative of abundant

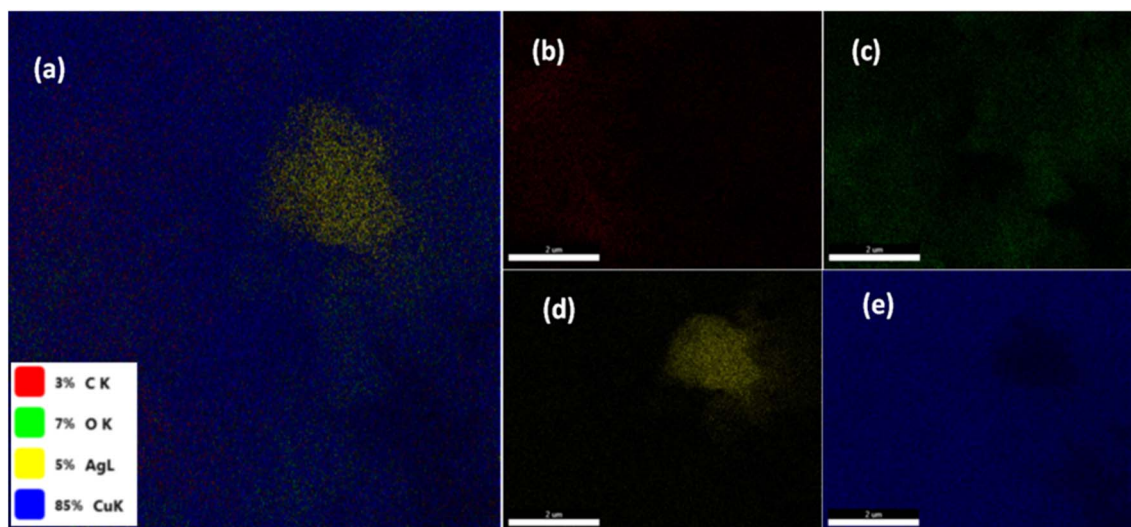


Fig. 2 EDX elemental mapping of silver doped CuO@GO composite. (a) Survey analysis (b) carbon (c) oxygen (d) silver and (e) copper.



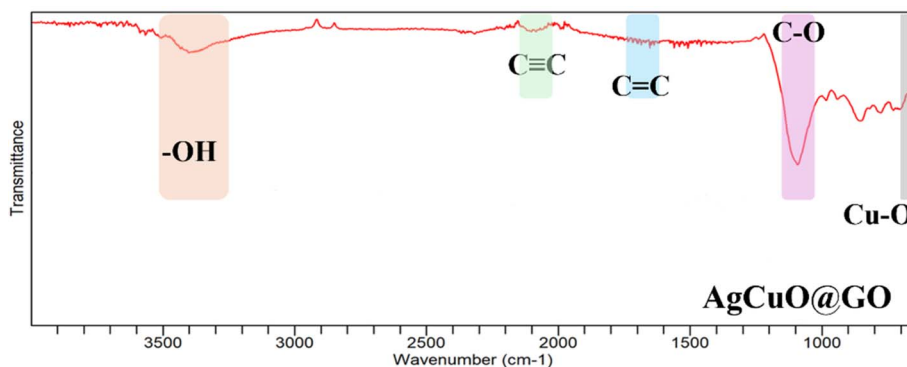


Fig. 4 FTIR spectra of Ag-doped CuO@GO.

oxygen-containing functional groups that arise due to the oxidative treatment of graphite during the GO synthesis. A broad absorption band centered around 3400 cm^{-1} corresponds to the O–H stretching vibrations of hydroxyl groups and intercalated water molecules.³⁹ The peak near 2130 cm^{-1} can be attributed to the C≡C stretching vibrations from residual hydrocarbons.

The prominent band at 1615 cm^{-1} is associated with the skeletal C=C stretching vibrations of the unoxidized graphitic domains or the adsorbed water's H–O–H bending mode. In addition, the peak around 1080 cm^{-1} is assignable to the alkoxy C–O stretching vibrations, reinforcing the presence of oxygenated moieties across GO sheets.⁴⁰

Notably, absorption bands emerge in the below 700 cm^{-1} region. These are attributed to the Cu–O stretching vibrations, confirming the incorporation of copper oxide nanoparticles.⁴¹ The presence of these vibrations substantiates the successful loading and chemical anchoring of CuO species onto the GO surface. Additionally, the overall reduction in band intensities in the CuO@GO spectrum relative to GO not only reflects the removal of oxygen functionalities but also indicates a strong metal support interaction between CuO and the GO matrix, essential for enhancing the composite's physicochemical properties. Thus, it confirms the successful synthesis of CuO@GO by highlighting the chemical transformation of GO into a reduced form and the effective incorporation of CuO nanoparticles, making the composite suitable for potential applications in catalysis, sensing, or energy storage.

3.2 Photocatalytic studies

The photocatalytic activity of Ag–CuO@GO was assessed through the degradation of MB dye under visible light irradiation. As shown in Fig. 5(a–c), intensity of the absorption peak of MB at 664 nm decreased over time, demonstrating efficient degradation of the dye. The NCs showed 75.7% MB degradation within 30 minutes at a catalyst concentration of 0.2 mg mL^{-1} . When the concentration was increased to 0.3 mg mL^{-1} , the degradation efficiency rose up to 96%, as shown in Fig. 5(d), representing excellent photocatalytic performance of NCs. The degradation kinetics followed a pseudo-first-order model, with a calculated rate constant (K_{app}) of 0.019 min^{-1} , confirming rapid pollutant removal.

The higher performance is due to the synergistic effects of Ag, CuO, and GO. Ag NPs enhance visible light absorption *via* surface plasmon resonance (SPR), while CuO helps electron–hole pair generation. GO acts as an electron acceptor, reducing recombination and facilitating the generation of reactive oxygen species (ROS) such as $\cdot\text{OH}$ and $\text{O}_2^{\cdot-}$, which are responsible for oxidative degradation of MB molecules.⁴² Fig. 5(e) presents the reusability of the Ag–CuO@GO composite for the degradation of MB dye in five consecutive cycles, indicating its stability. The observed decrease in degradation efficiency is due to the blockage of active sites by adsorbed intermediate species and the minimal mechanical loss of catalyst during the recovery process between cycles. The results highlight the potential of Ag–CuO@GO as a highly efficient photocatalyst for environmental applications.

3.3 Electrochemical sensing

3.3.1 Electrochemical response of DA on Ag–CuO@GO electrode. Fig. 6(a) illustrates the cyclic voltammetry (CV) response of the fabricated composite electrode in the presence of increasing concentrations of dopamine (DA), ranging from 0 mM to 1.1 mM in 0.2 mM intervals. A distinct anodic peak appears near $+0.36\text{ V}$, corresponding to the oxidation of dopamine to dopamine-*o*-quinone. The cathodic peak observed around 0 V represents the reverse reduction process, indicating a quasi-reversible redox couple. As the dopamine concentration increases, the redox peak currents gradually increase, demonstrating the excellent electrocatalytic activity of the composite material toward dopamine oxidation. The enhanced electrochemical performance can be attributed to the synergistic combination of silver and copper oxide nanoparticles uniformly anchored on the graphene oxide matrix. The CuO offers redox-active sites, while Ag nanoparticles contribute to improved electrical conductivity and enhanced electron mobility. The presence of graphene oxide ensures a high surface area, favoring increased dopamine adsorption and electron exchange.⁴³ The integration of these components falls into a porous and conductive framework, promoting effective redox interaction with dopamine. As shown in the calibration plot derived from Fig. 6(b), a linear range of 0 to 1.1 mM was established for dopamine detection, with a regression coefficient of ($R^2 = 0.98$) confirming a strong linear correlation, also



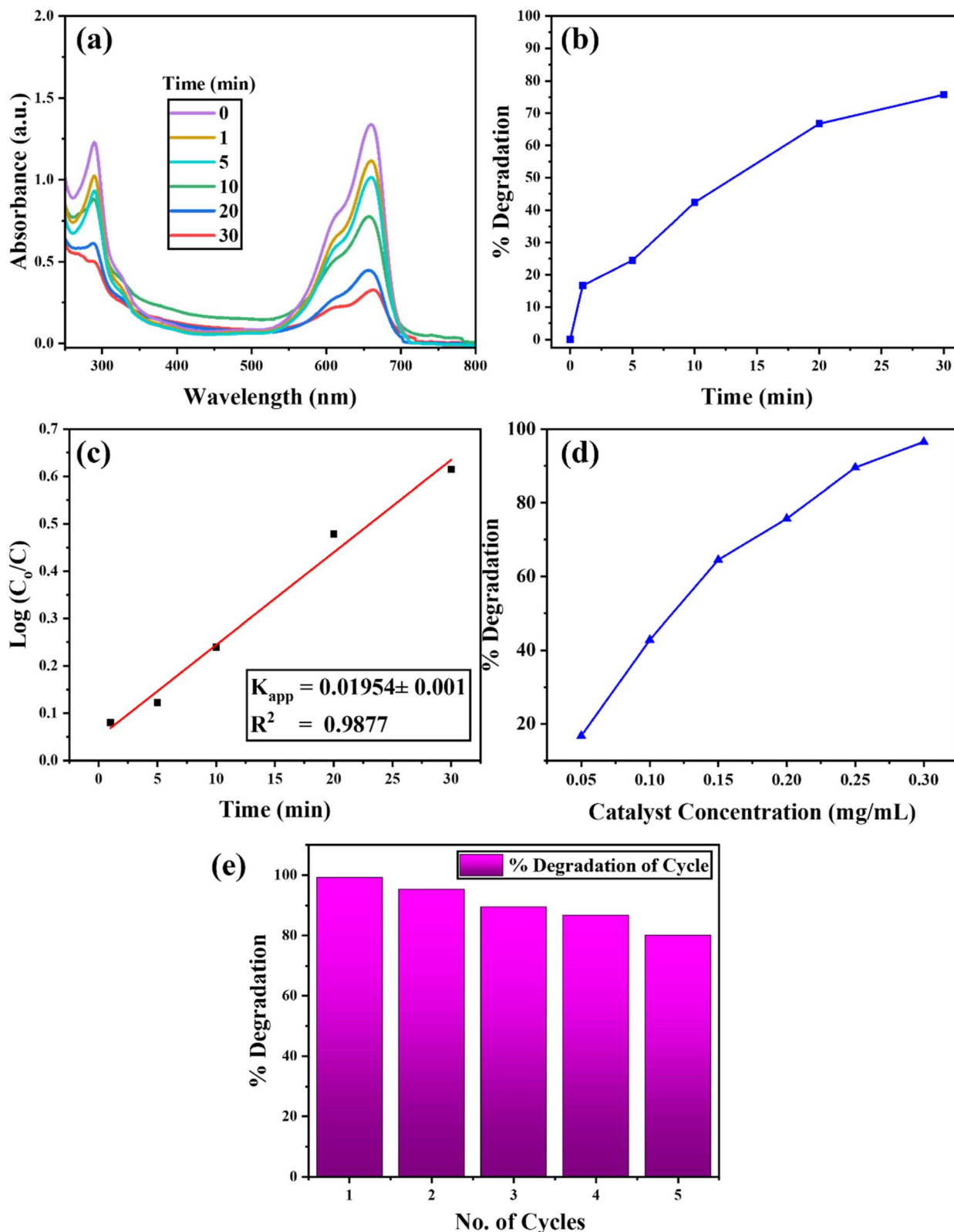


Fig. 5 (a) UV-vis spectra showing time-dependent decrease in absorbance. (b) % degradation of the dye (c) apparent rate constant of dye degradation (d) effect of the concentration of catalyst (e) reusability studies of the catalyst against MB via consecutive cycles.

enabling the electrode to be suitable for the quantitative determination of dopamine in similar ranges. The limit of detection (LOD) was determined to be $23.6 \mu\text{M}$, and the limit of

quantification (LOQ) was calculated as $71 \mu\text{M}$, respectively. Furthermore, the sensitivity of the sensor was calculated to be $3.43 \text{ mA cm}^{-2} \text{ mM}^{-1}$, indicating the system's ability to produce



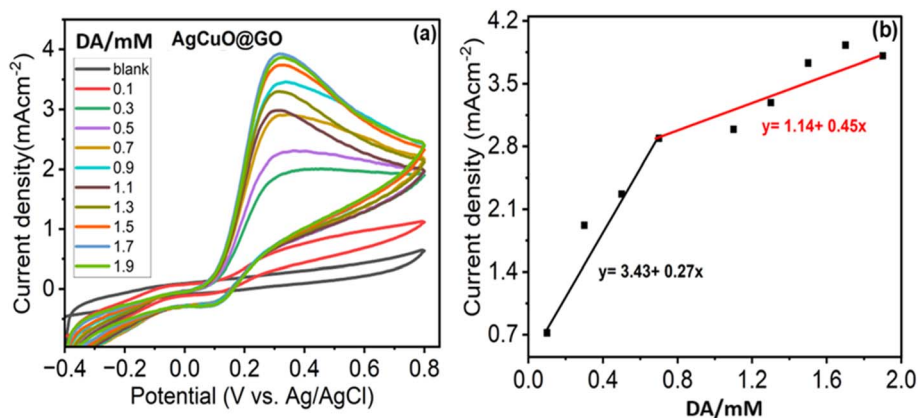


Fig. 6 (a) Cyclic voltammogram for Ag–CuO@GO modified at the glassy carbon electrode (GCE) electrode with different concentration of dopamine in phosphate buffer solution (PBS) and (b) corresponding linear calibration plot.

a strong electrochemical response per unit concentration per electrode area. The linearity also suggests diffusion-controlled behavior, implying that the dopamine molecules diffuse toward the electrode surface and undergo efficient electron transfer upon interaction with the sensing material.

The high sensitivity of the Ag–CuO@GO electrode reflects its superior catalytic activity and efficient electron transfer at the analyte–electrode interface. In comparison with bare glassy carbon electrode (GCE) as shown in the Fig. 7, the sensitivity is far behind with the value of $0.394 \text{ mA cm}^{-2} \text{ mM}^{-1}$ reflected from the calibration curves in Fig. 7(b). The reproducible and stable CV response underscores its reliability for dopamine detection.

Beyond sensing, the same composite's redox-active components and surface reactivity also contribute to its antimicrobial efficacy, highlighting its dual-functional potential in both bioelectrochemical diagnostics and microbial inhibition.

A diffusion-controlled electrochemical process is indicated by the cyclic voltammetry (CV) plots in Fig. 8(a), which shows that the current density at the Ag–CuO@GCE electrode increases as the scan rate (SR) rises from 50 to 130 mV s^{-1} . This implies that the charge transfer is improved at faster scan rates because of the increased flux of electroactive species towards

the electrode surface and that the redox reaction kinetics are comparatively quick. Capacitive behavior with faradaic contributions is further implied by the quasi-reversible nature of the redox peaks moving with scan rate. The Ag–CuO nanostructure's surface reconfiguration or electrochemical activation is indicated by the steady decline in current density seen in the CV curves over fifty consecutive cycles in Fig. 8(b). This investigation showed that the fabricated composite electrode could be used for several times to assess the analyte including glucose and related biomolecules.

This improvement is probably the result of enhanced electrolyte penetration, greater electron conductivity and improved electroactive surface area all of which work together to gradually expose catalytically active areas improving the electrode's redox performance.

The data presented in Table 1 substantiate the electrochemical competence of the Ag–CuO@GO sensor toward electrochemical detection of dopamine. The low LOD signifies the sensor's capacity to detect trace dopamine levels, essential for accurate monitoring in biological or clinical matrices. The wide linear range enables detection across physiological dopamine concentrations, while the high sensitivity affirms the material's catalytic strength. Overall, these metrics validate the

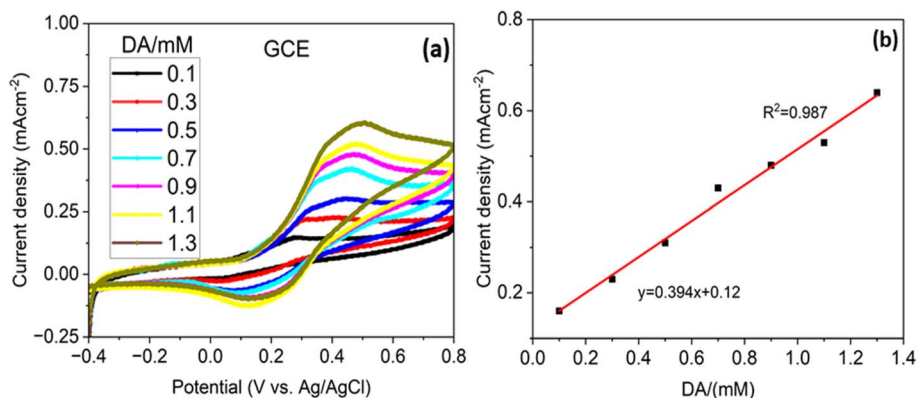


Fig. 7 (a) Cyclic voltammogram for bare GCE electrode with different concentration of dopamine in PBS and (b) its linear calibration plot.

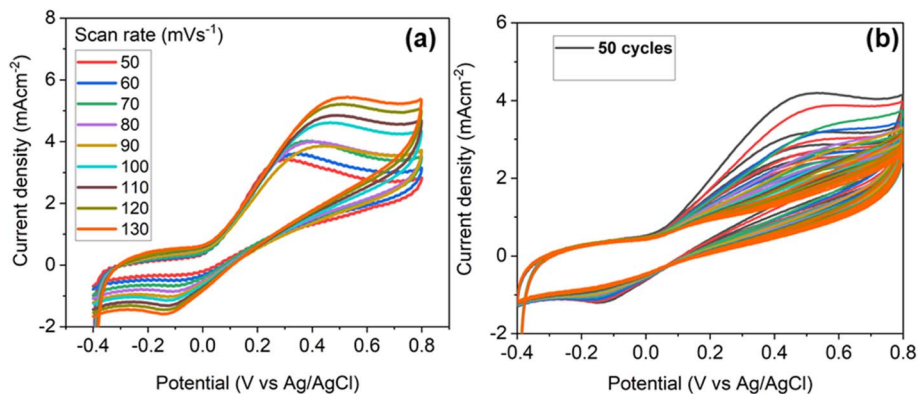


Fig. 8 Cyclic voltammograms with (a) different scan rates (50–130 mV s^{-1}) at Ag–CuO@GO modified GCE under fixed concentration and (b) CV cycles (50) for the stability test with fixed concentration and scan rate.

Table 1 Electrochemical performance parameters for dopamine detection using Ag–CuO@GO electrode

Electrode	Analyte	Sensitivity ($\text{mA cm}^{-2} \text{mM}^{-1}$)	LOD (μM)	LOQ (μM)	LR (mM)
Ag–CuO@GO	Dopamine	3.43	23.6	71	0.1–0.7 0.7–1.9
GCE	Dopamine	0.394	124.7	372	0.1–1.3

electrode's performance and highlight its prospective use in advanced electrochemical sensing applications.

3.3.2 Chronoamperometric response. Fig. 9(a and b) present the chronoamperometric response and corresponding calibration behavior of the Ag–CuO@GO modified electrode for dopamine (DA) detection under successive additions of the analyte. As shown in Fig. 8(a), each incremental addition of dopamine (ranging from 0.4 mM to 1.0 mM) induces a distinct and immediate increase in current, followed by gradual stabilization, consistent with a diffusion-controlled oxidation process. The well-resolved and reproducible current highlights the rapid electron transfer kinetics and strong electrocatalytic interaction between dopamine and the nanocomposite surface. The corresponding calibration curve in Fig. 9(b) demonstrates

a clear linear relationship between the steady-state current and dopamine concentration, with a regression equation $I (\mu\text{A}) = 72.97C + 0.90$ and a correlation coefficient ($R^2 = 0.97$). This linearity confirms the electrode's quantitative sensing capability across the tested range (0.4–1.0 mM), further substantiated by its low detection and quantification with a higher sensitivity ($72.97 \mu\text{A cm}^{-2} \text{mM}^{-1}$ for chrono). The chronoamperometric data affirm that the Ag–CuO@GO electrode exhibits reliable, fast-response behavior and high analytical performance, positioning it as a promising platform for real-time neurotransmitter monitoring in complex media.

High selectivity and stability are demonstrated by the Ag–CuO@GCE electrode's amperometry response to dopamine (DA) in the presence of common interfering species, such as

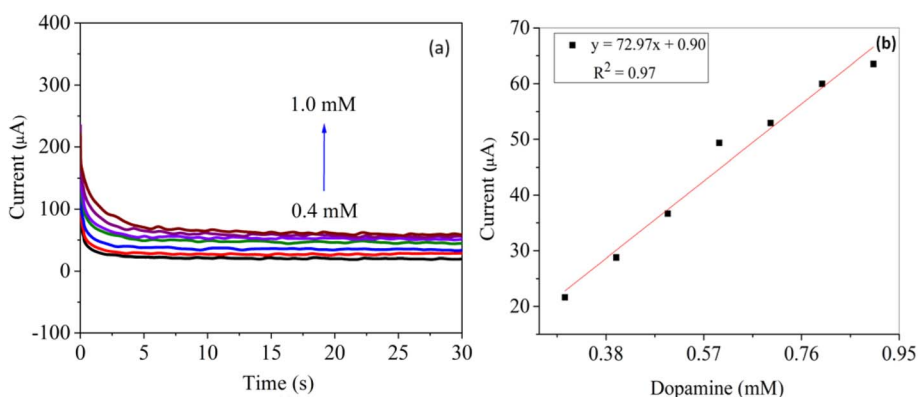


Fig. 9 (a) Chronoamperometric response of Ag–CuO@GO electrode for dopamine (0.4–1.0 mM) under the redox potential applied and (b) its linear calibration plot.



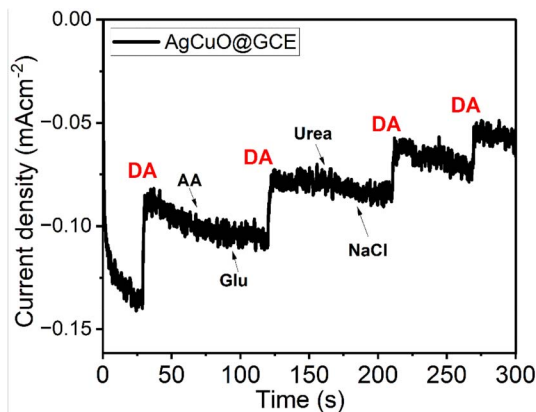


Fig. 10 Staircase voltammogram at the Ag-doped CuO@GO modified GCE electrode exhibiting the effect of interference study.

ascorbic acid (AA), glucose (Glu), urea, and NaCl (Fig. 10). As a result of DA's distinct catechol structure and particular adsorption behavior, the electro-oxidation of DA is selectively facilitated by the synergistic redox activity and surface chemistry of Ag and CuO. Despite being electroactive, AA and Glu generate much lower current responses most likely as a result of kinetic impediment, electrostatic repulsion or weak contact with the electrode surface. Due to their electrochemical inactivity at the specified voltage, urea and NaCl produce very small current changes indicating very little interference. The electrode's great affinity and good anti-interference performance-essential characteristics for selective DA sensing in biological environments are highlighted by the noticeable and rapid increase in current that occurs with each reintroduction of DA.

3.3.3 Square wave voltammetry. The electrochemical performance of AgCuO@GO modified GCE electrode toward dopamine detection was evaluated using square wave voltammetry (SWV) as demonstrated in Fig. 11(a). The SWV profile exhibit a distinct oxidation peak at 0.12 V (vs. Ag/AgCl) which corresponds to electrochemical oxidation of dopamine. With increasing DA concentration from 10 to 100 μM a progressive enhancement in peak current density is observed, indicating

a strong concentration dependent response. The corresponding calibration curve (Fig. 11(b)) demonstrates a linear relationship between the peak current density and DA concentration, expressed by the equation $y = 0.013x$ with correlation coefficient (R^2) of 0.98 signifying excellent linearity. The sensitivity of electrode is reports as $13 \text{ mA cm}^{-2} \mu\text{M}^{-1}$, additionally the LOD is 6 μM reflecting the lowest concentration of dopamine that can be accurately detected using this sensor.

3.4 Antimicrobial activity

The antibacterial activity of Ag-CuO@GO nanocomposite demonstrated in Table 2 against both *E. coli* and *S. aureus*, with a clear response. The larger zones of inhibition observed at higher loadings of 10 μL suggest that the efficacy of nanocomposite is influenced by concentration. This is due to increased availability of ROS. The greater exposure of *E. coli* compared to *S. aureus* may be due to structural differences in their cell membrane. *E. coli*, with its thinner peptidoglycan layer and outer membrane, may allow easier interaction with ROS, whereas the thick, cross-linked peptidoglycan layer of *S. aureus* provides a stronger barrier,⁴⁴ necessitating higher concentration of ROS for effective disruption.

The antimicrobial mechanism of Ag-CuO@GO is based on the ability to generate ROS. These oxidative agents induce severe cellular damage, such as lipid peroxidation, protein oxidation, and DNA strand breaks, leading to cell death. The GO matrix enhances this activity by helping electron transfer and stabilizing the metal nanoparticles for ROS generation.

Table 2 Antibacterial activity via disc diffusion method using Ag-CuO@GO nanocomposite

Sample	Loading (1 mg mL^{-1})	Zone of inhibition	
		<i>E. coli</i>	<i>S. aureus</i>
Ag-CuO@GO	5 μL	$18 \pm 0.1 \text{ mm}$	$12 \pm 0.1 \text{ mm}$
	10 μL	$20 \pm 0.1 \text{ mm}$	$17 \pm 0.1 \text{ mm}$
Streptomycin	10 μL	$40 \pm 0.1 \text{ mm}$	$40 \pm 0.1 \text{ mm}$

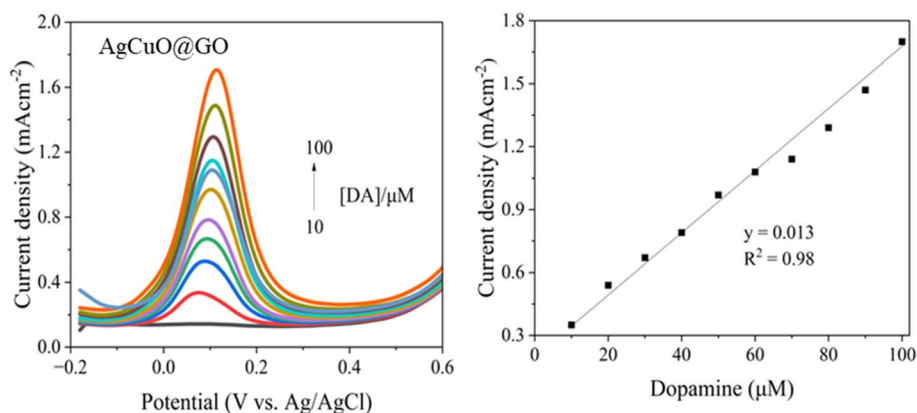


Fig. 11 Square wave voltammograms of AgCuO@GO modified GCE electrode toward dopamine detection at varying concentration, and (b) the corresponding calibration plot.



Although Ag–CuO@GO showed strong antibacterial activity, it was less active than the standard streptomycin. However, the ROS facilitated mechanism make Ag–CuO@GO as a valuable candidate against antibiotic-resistant strains, where conventional antibiotics may fail. Future work should focus on optimizing the synthesis to enhance ROS yield, evaluating biocompatibility, and exploring synergistic effects with existing antibiotics to maximize its therapeutic potential.

4. Conclusion

In this study, an Ag–CuO nanocomposite decorated on graphene oxide (Ag–CuO@GO) was effectively synthesized *via* a wet-chemical method and comprehensively characterized using multiple analytical techniques. The synergistic effect of Ag, CuO, and GO offered enhanced charge separation, conductivity, and a high-surface-area for effective electron transfer. Electrochemical studies verified excellent sensing performance for dopamine with quick response and low limit of detection, confirming applicability of Ag–CuO@GO in biosensing. In addition, the nanocomposite revealed notable photocatalytic activity, attaining efficient MB degradation under direct sunlight. Ag–CuO@GO showed tunable degradation efficiency by changing catalyst concentration and following pseudo-first-order kinetics. In addition to electrochemical and photocatalytic methods, the Ag–CuO to GO composite showed strong antibacterial features, which is attributed to the inherent biocidal nature of silver and copper(II) oxide, which increases its potential real-world applications. Combined, these findings make Ag–CuO and GO a highly multifunctional nanomaterial with significant possibilities in electrochemical sensing, environmental remediation settings, as well as with its antibacterial benefits. While demonstrating the efficacy of the Ag–CuO@GO composite, this study is limited to a single Ag doping concentration and the use of GO as the sole carbon support. Future work should involve a systematic variation of Ag dopant levels and extend to other carbon matrices like rGO, CNTs, and carbon nano-onions to identify the most synergistic and active catalyst configuration for multifunctional activity.

Conflicts of interest

There are no conflict to declare.

Data availability

All relevant data supporting the findings of this study are included in the article. Additional datasets generated and/or analyzed during the current study are available from the corresponding author upon reasonable request.

Acknowledgements

Authors are highly thankful to the Department of Biology, Al-Baha University, Al-Baha, Saudi Arabia for the financial support of this work.

References

- 1 Y. Fu, *et al.*, Applications of nanomaterial technology in biosensing, *J. Sci.: Adv. Mater. Devices*, 2024, **9**(2), 100694.
- 2 C. Cha, S. R. Shin, N. Annabi, M. R. Dokmeci and A. Khademhosseini, Carbon-Based Nanomaterials: Multifunctional Materials for Biomedical Engineering, *ACS Nano*, 2013, **7**, 2891–2897.
- 3 D. M. Tobaldi, *et al.*, Hybrid Noble-Metals/Metal-Oxide Bifunctional Nano-Heterostructure Displaying Outperforming Gas-Sensing and Photochromic Performances, *ACS Omega*, 2018, **3**(8), 9846–9859.
- 4 M. Saleh, *et al.*, Comprehensive review of Carbon-based nanostructures: Properties, synthesis, characterization, and cross-disciplinary applications, *J. Ind. Eng. Chem.*, 2025, **146**, 176–212.
- 5 A. Sahai, *et al.*, Structural, vibrational and electronic properties of CuO nanoparticles synthesized *via* exploding wire technique, *Ceram. Int.*, 2018, **44**(2), 2478–2484.
- 6 K. Tamil Thendral, M. Amutha and R. Ragunathan, Versatile biopolymer-functionalized copper cobalt oxide nanocomposite (Ch/CuCo2O4): Synthesis and applications in antibacterial, anticancer, and photocatalysis, *Ceram. Int.*, 2024, **50**(10), 16929–16939.
- 7 M. Imran, *et al.*, Excellent successive photo-induced degradation of tetracycline using CuO/g-C3N4 nanocomposites: Synergistic effects of CuO integration and H2O2 in a photo-Fenton system, *J. Taiwan Inst. Chem. Eng.*, 2025, **171**, 106068.
- 8 B. Uma, *et al.*, Controlled synthesis of (CuO-Cu2O)Cu/ZnO multi oxide nanocomposites by facile combustion route: A potential photocatalytic, antimicrobial and anticancer activity, *Ceram. Int.*, 2021, **47**(10), 14829–14844.
- 9 K. Atacan, *et al.*, Fabrication of silver doped different metal oxide nanoparticles and evaluation of their antibacterial and catalytic applications, *Appl. Surf. Sci. Adv.*, 2021, **6**, 100156.
- 10 J. Singh and R. K. Soni, Efficient charge separation in Ag nanoparticles functionalized ZnO nanoflakes/CuO nanoflowers hybrids for improved photocatalytic and SERS activity, *Colloids Surf., A*, 2021, **626**, 127005.
- 11 X. Fan, L. Yahia and E. Sacher, Antimicrobial Properties of the Ag, Cu Nanoparticle System, *Biology*, 2021, **10**(2), 137.
- 12 C.-H. Chen, *et al.*, Effective Synthesis of Highly Oxidized Graphene Oxide That Enables Wafer-scale Nanopatterning: Preformed Acidic Oxidizing Medium Approach, *Sci. Rep.*, 2017, **7**(1), 3908.
- 13 A. H. Chisty, Enhanced epoxy/GO composites mechanical and thermal properties by removing air bubbles with shear mixing and ultrasonication, *ChemistrySelect*, 2019, **4**(38), 11417–11425.
- 14 X. Duan, W. Liu and J. Guo, Microwave-Field-Optimized GO/TiO₂ Nanomaterials for Enhanced Interfacial Charge Transfer in Photocatalysis, *Nanomaterials*, 2024, **14**(23), 1912.
- 15 P. Ponnarasi and G. Mahalakshmi, Ag-doped CuO nanoparticles embedded reduced graphene oxide



- nanocomposite from Punica granatum peel extract and evaluation of their photocatalytic activity and antimicrobial potential, *Chem. Phys. Impact*, 2024, **8**, 100632.
- 16 R. Ahmadi, *et al.*, Evaluation of antibacterial behavior of *in situ* grown CuO-GO nanocomposites, *Mater. Today Commun.*, 2021, **28**, 102642.
- 17 A. T. Mosleh, *et al.*, Performance of Ag-doped CuO nanoparticles for photocatalytic activity applications: Synthesis, characterization, and antimicrobial activity, *Discover Nano*, 2024, **19**(1), 166.
- 18 N. Roy, S. Yasmin and S. Jeon, Effective electrochemical detection of dopamine with highly active molybdenum oxide nanoparticles decorated on 2, 6 diaminopyridine/reduced graphene oxide, *Microchem. J.*, 2020, **153**, 104501.
- 19 W. Xu, Y. Chen and Y. J. C. Liu, Electrochemical Enzyme-Free Dopamine Sensor Based on Prussian Blue Analogues Oxides and MWCNTs, *ChemistrySelect*, 2024, **9**(41), e202403603.
- 20 S. Paravati, A. Rosani, S. J. Warrington, *Physiology, catecholamines in StatPearls*, StatPearls Publishing, 2024.
- 21 K. Amarnath, *et al.*, Electrochemical Detection of Dopamine and Uric Acid with Annealed Metal–Organic Framework/MXene (CuO/C/Ti₃C₂Tx) Nanosheet Composites for Neurotransmitter Sensing, *ACS Appl. Nano Mater.*, 2025, **8**(24), 12661–12675.
- 22 A. Barhoum, *et al.*, Modern designs of electrochemical sensor platforms for environmental analyses: Principles, nanofabrication opportunities, and challenges, *Trends Environ. Anal. Chem.*, 2023, **38**, e00199.
- 23 L. Ding, *et al.*, Visible-light-driven photoelectrochemical biosensor for sulfadimethoxine detection based on bismuth-ternary hybrid heterostructure, *Microchem. J.*, 2025, **212**, 113440.
- 24 R. M. Ahmed and E. Al-Bermamy, Tuning the optical absorption and band gap of hydrogel methylcellulose loaded using hybrid Fe₃O₄@GO nanomaterials for optoelectronic and antibacterial activity, *J. Opt.*, 2024, DOI: [10.1007/s12596-024-02204-2](https://doi.org/10.1007/s12596-024-02204-2).
- 25 Z. Wang, *et al.*, An enhanced ultra-fast responding ethanol gas sensor based on Ag functionalized CuO nanoribbons at room-temperature, *J. Mater. Sci.: Mater. Electron.*, 2018, **29**, 16654–16659.
- 26 G. A. Sotiriou and S. E. Pratsinis, Engineering nanosilver as an antibacterial, biosensor and bioimaging material, *Curr. Opin. Chem. Eng.*, 2011, **1**(1), 3–10.
- 27 M. Devaraji, P. V. Thanikachalam and K. Elumalai, The potential of copper oxide nanoparticles in nanomedicine: A comprehensive review, *Biotechnol. Notes*, 2024, **5**, 80–99.
- 28 D. Sharma, *et al.*, Insight into the biosensing of graphene oxide: Present and future prospects, *Arabian J. Chem.*, 2016, **9**(2), 238–261.
- 29 T. Shahnaz and G. Hayder, Exploring graphene's antibacterial potential for advanced and sustainable solutions in water treatment, *J. Water Process Eng.*, 2023, **56**, 104530.
- 30 W. Cheng, *et al.*, The study on nanostructural evolution of CuO/Graphene oxide nanocomposite during the first discharge processes, *Mater. Chem. Phys.*, 2021, **260**, 124157.
- 31 M. A. Barakat, *et al.*, A novel CuO–Cu₂O/Ag–Ag₃PO₄ nanocomposite: Synthesis, characterization, and its application for 2-chlorophenol decontamination under visible light, *J. Taiwan Inst. Chem. Eng.*, 2020, **115**, 208–217.
- 32 L. Yang, *et al.*, Silver nanowires: from synthesis, growth mechanism, device fabrications to prospective engineered applications, *Eng. Sci.*, 2023, **23**(3), 808.
- 33 V.-D. Hodoroaba, Chapter 4.4 - Energy-dispersive X-ray spectroscopy (EDS), in *Characterization of Nanoparticles*, ed. V.-D. Hodoroaba, W. E. S. Unger and A. G. Shard, Elsevier, 2020. pp. 397–417.
- 34 K. H. Helfferich, *et al.*, Quantifying elemental colocation in nanostructured materials using energy-dispersive X-ray spectroscopy, *Ultramicroscopy*, 2025, **271**, 114123.
- 35 A. O. Ilori and O. Ajanaku, Characteristics of Synthesized Copper Oxide (CuO) Nanoparticles using Maize Husks: A Green Chemistry Approach, *Int. J. Environ. Eng. Educ.*, 2022, **4**(1), 1–4.
- 36 X.-Y. Zhu, *et al.*, Controlled fabrication of well-dispersed AgPd nanoclusters supported on reduced graphene oxide with highly enhanced catalytic properties towards 4-nitrophenol reduction, *J. Colloid Interface Sci.*, 2018, **516**, 355–363.
- 37 G. Vinodha, P. Shima and L. Cindrella, Mesoporous magnetite nanoparticle-decorated graphene oxide nanosheets for efficient electrochemical detection of hydrazine, *J. Mater. Sci.*, 2019, **54**(5), 4073–4088.
- 38 M. Farooq, Phytoassisted synthesis of CuO and Ag–CuO nanocomposite, characterization, chemical sensing of ammonia, degradation of methylene blue, *Sci. Rep.*, 2024, **14**(1), 1618.
- 39 F. Ali, *et al.*, Ag and Zn doped TiO₂ nano-catalyst synthesis via a facile green route and their catalytic activity for the remediation of dyes, *J. Mater. Res. Technol.*, 2023, **23**, 3626–3637.
- 40 F. Ali, *et al.*, Silver and zinc oxide decorated rGO nanocomposites as efficient electrocatalysts towards oxygen evolution reactions under alkaline conditions, *Diamond Relat. Mater.*, 2024, **148**, 111378.
- 41 J. H. Taha, N. K. Abbas and A. A. Al-Attaqchi, Green synthesis and evaluation of copper oxide nanoparticles using fig leaves and their antifungal and antibacterial activities, *J. Drug Delivery Sci. Technol.*, 2020, **10**, 378–382.
- 42 I. Bayach, *et al.*, Fabrication of Binary Metal Selenide@CNTs based Nanocomposite for Enhanced Antimicrobial Activity and Rapid Photocatalytic Degradation of Organic Pollutants, *Colloids Surf., B*, 2025, 114845.
- 43 R. Aukštakojytė, *et al.*, Bismarck brown-assisted hydrothermal synthesis of nitrogen-modified reduced graphene oxide for selective electrochemical detection of dopamine, *Surf. Interfaces*, 2024, **46**, 104041.
- 44 S. Mehmood, *et al.*, Development and characterization of glutaryl thiourea crosslinked novel hydrogel; a detailed analysis of biocompatibility, angiogenesis, and antibacterial potential, *React. Funct. Polym.*, 2025, 106313.

